


Lambertian illumination of dielectric scattering media with monochromatic light

Felix Ott* and Alwin Kienle

*Institut für Lasertechnologien in der Medizin und Meßtechnik an der Universität Ulm, Helmholtzstr. 12, D-89081 Ulm, Germany
and Universität Ulm, Albert-Einstein-Allee 11, D-89081 Ulm, Germany* (Received 17 January 2022; revised 15 March 2022; accepted 18 March 2022; published 30 March 2022)

We study the Lambertian illumination of dielectric media with monochromatic light by numerically solving Maxwell's equations in three dimensions. We compute the average energy density inside spherical and cubic objects with a uniform refractive index. The Lambertian illumination of objects with uniform refractive index reproduces the known enhancement of the average energy density equal to the third power of the refractive index if the surface is sufficiently textured. Furthermore, inhomogeneous refractive index distributions with scattering areas much smaller than the wavelength, of the order of the wavelength, and larger than the wavelength are studied. The average energy density inside these media is compared to effective medium theories. Our investigation shows that the average energy density enhancement inside scattering media with scatterers much smaller than the wavelength can be modeled accurately with effective medium approximations.

DOI: [10.1103/PhysRevA.105.033528](https://doi.org/10.1103/PhysRevA.105.033528)**I. INTRODUCTION**

Understanding light propagation inside complex media is of great interest in many different areas of research and engineering science. Examples are imaging under complex conditions such as for noninvasive biological imaging [1] or improving photovoltaics for energy harvesting in engineering science [2]. In general, to understand light propagation in a specific situation theoretically, it is necessary to consider the detailed material properties and the illumination scenario. If the illumination is isotropic and uniform, which is often termed Lambertian illumination, some general conclusions for the light field can be made. For example, Lambertian illumination of a planar semi-infinite surface results in a Lambertian distribution of the reflected light [3]. The light distribution inside objects, such as textured sheets, with refractive index n was studied by Yablonoitch in the context of light trapping in solar cells [4]. He showed that for ergodic systems, the intensity enhancement inside the medium is equal to n^2 , and if absorbing regions inside the medium are present, the absorption enhancement cannot exceed $\sim 4n^2$. This limit was derived by statistical geometrical optics. Later it was shown that this limit can be surpassed in the context of nanophotonic light trapping in solar cells [5]. Closely related to this subject is the phenomenon of mean path-length invariance of random walks [6], which is a generalization of the mean chord-length theorem [7]. This invariance property states that the mean path length across a finite nonabsorbing system is only dependent on the volume and surface of the system and not on the characteristics of the scattering process. A similar invariance property for wave scattering through turbid media could also be found in resonant structures as well as in the ballistic, chaotic, and localized scattering regime [8].

Recently, the mean path-length invariance has been observed for light in the visible range for different scattering media [9]. Theoretical investigations based on the radiative transfer equation for simple dielectric scattering objects, such as a slab or a sphere filled with scatterers, under Lambertian illumination showed that this mean path-length invariance scaled by a factor n^2 , which is related to the intensity enhancement due to Yablonoitch, still holds [10,11].

The theoretical investigations in the mentioned publications concerning Lambertian illumination are often based on either ray optics, radiative transfer theory, numerical solutions of the Helmholtz equation inside a two-dimensional (2D) waveguide geometry, or statistical temporal coupled-mode theory for periodic structures. In our study we make use of rigorous numerical solutions to Maxwell's equations in three dimensions to obtain the electromagnetic field distribution inside dielectric objects which are subject to Lambertian illumination. We investigate the energy density distribution inside the objects. We have to emphasize that we do not investigate the intensity of the light, which is often either defined as proportional to the electric field squared or the absolute value of the Poynting vector. These definitions of the intensity can yield different results, especially for Lambertian illumination. The use of the absolute value of the Poynting vector as a measure of intensity would result in a vanishing average intensity in regions under Lambertian illumination. We believe that the average energy density of the electromagnetic field is in this context more appropriate as it can be directly linked to quantities of the radiative transfer theory without a scaling factor [12,13].

In Sec. II we first describe the term Lambertian illumination and the consequences for the light distribution inside dielectric scattering objects. Furthermore, the simulation approach to obtain the electromagnetic fields and the energy density distribution is described. Subsequently, the results are presented and discussed in Sec. III, where first finite media

*Corresponding author: felix.ott@ilm-ulm.de

with a uniform refractive index are investigated (Sec. III A), and second, volume scattering media composed of scatterers with different sizes, refractive indices, and volume fractions (Sec. III B). Finally, a summary and a conclusion can be found in Sec. IV.

II. THEORY AND SIMULATION APPROACH

A. Lambertian illumination

Lambertian illumination is the isotropic and homogeneous illumination of a medium. Lambertian illumination of an ergodic system guarantees that all modes are occupied in equilibrium. If the medium is a dielectric and has a uniform refractive index n , the energy density $w(\omega)$ in a small frequency band $\omega d\omega$ inside the object is equal to that of the blackbody radiation in a vacuum multiplied by a factor of n^3 [14,15]. In the small frequency band it is assumed that the refractive index is constant. This result can also be derived based on fluctuating fields [14]. It has to be mentioned that in order to obtain the intensity enhancement of n^2 the intensity is defined as $I \equiv wv_g$, with the group velocity v_g of light inside the medium [4]. In our case, the illumination comprises only one frequency ω and is therefore monochromatic. The enhancement of the energy density for a single frequency is still valid if the illuminated object is also nonabsorbing [15].

For Lambertian illumination with only one frequency, the light field in a vacuum is a three-dimensional speckle pattern. It is similar to the interference of many plane waves traveling in all directions. To obtain a meaningful average energy density $\langle w \rangle$ of a Lambertian monochromatic light field it is necessary to average over a sufficiently large area containing many speckles of size $\sim \lambda$. The average energy density inside a vacuum is denoted by w_0 . Consequently, the average energy density enhancement inside homogeneous dielectric media is

$$\frac{\langle w \rangle}{w_0} = n^3. \quad (1)$$

In the case of a dielectric medium with a nonuniform refractive index $n(\mathbf{r})$ Eq. (1) is still valid locally if the refractive index slowly varies over areas much larger than the wavelength [15]. Therefore, we can obtain the average energy density $\langle w \rangle$ inside a scattering medium by averaging the local energy density $w(\mathbf{r})$ over its volume V . The average energy density enhancement is calculated as

$$\frac{\langle w \rangle}{w_0} = \frac{\int_V w(\mathbf{r}) dV}{V w_0} = \frac{\int_V n(\mathbf{r})^3 dV}{V}. \quad (2)$$

If the medium is composed of N discrete scatterers or subvolumes with a uniform refractive index, the integral in Eq. (2) can be replaced by a sum over all subvolumes

$$\frac{\langle w \rangle}{w_0} = \sum_i^N n_i^3 f_{V,i}, \quad (3)$$

where $f_{V,i}$ denotes the volume fraction and n_i the refractive index of the i th subvolume inside the medium. For a discrete medium composed of only two discrete refractive indices n_1 and n_2 , where one type has a volume concentration of f_V ,

Eq. (3) reduces to

$$\frac{\langle w \rangle}{w_0} = f_V n_1^3 + (1 - f_V) n_2^3. \quad (4)$$

If the local change in the refractive index varies much faster than the wavelength, the above equations are not valid anymore. However, we can approximate the inhomogeneous medium with fast variations in the refractive index as a homogeneous medium with an effective refractive index denoted by \tilde{n} . The most common theories from which an effective refractive index can be obtained are the Maxwell-Garnett (MG) and the Bruggeman (BG) effective medium approximations [16,17]. From these theories, one can calculate an effective permittivity dependent on the permittivity and volume fraction of its components. Effective medium theories can improve the modeling of light scattering of colloidal aggregates [18] but also may have their limitations [19]. We rewrite the equations in terms of the refractive index, which is related in the case of nonmagnetic media to the permittivity ϵ by $n = \sqrt{\epsilon/\epsilon_0}$, where ϵ_0 is the vacuum permittivity. For a two-component system with refractive indices n_1 and n_2 and volume fraction of component 1, f_V (component 2 has the volume fraction of $1 - f_V$), the Maxwell-Garnett approximation gives an effective refractive index of

$$\tilde{n}_{\text{MG}} = \left(\frac{1 + 2f_V \frac{n_1^2 - n_2^2}{n_1^2 + 2n_2^2}}{1 - f_V \frac{n_1^2 - n_2^2}{n_1^2 + 2n_2^2}} \right)^{1/2}. \quad (5)$$

n_2 is often called the refractive index of the host medium. From the effective medium approximation of Bruggeman, one can obtain an effective refractive index with the following equation:

$$\tilde{n}_{\text{BG}} = \frac{1}{2} \sqrt{(b + \sqrt{8n_1 n_2 + b^2})}, \quad (6)$$

with $b = n_1^2(3f_V - 1) + n_2^2(2 - f_V)$. Both theories assume that the inclusions are spherical and the field inside the inclusion is homogeneous. This is equivalent to the statement that the inclusions are much smaller than the wavelength. We can also obtain an ‘‘effective’’ refractive index by averaging over the permittivity or the refractive index inside the inhomogeneous dielectric medium. These approximations are heuristic approaches and the formulas are not derived from first principles. Volumetric averaging over the permittivity of a two-component medium gives

$$\tilde{n}_{\epsilon, \text{avg}} = \sqrt{f_V n_1^2 + (1 - f_V) n_2^2}, \quad (7)$$

while averaging over the refractive index gives

$$\tilde{n}_{\text{avg}} = f_V n_1 + (1 - f_V) n_2. \quad (8)$$

We suggest to use Eq. (1) with an effective refractive index to obtain the average energy density enhancement in inhomogeneous dielectric media with scattering volumes much smaller than the wavelength.

B. Classical electromagnetism and numerical simulation

In classical electromagnetism, light can be described by the complex electric vector field $\mathbf{E}(r, t)$ and the complex

magnetic vector field $\mathbf{H}(\mathbf{r}, t)$. Both fields are dependent on position \mathbf{r} and time t . For a specific complex refractive index distribution $n(\mathbf{r})$ and incident field, $\mathbf{E}(\mathbf{r}, t)$ and $\mathbf{H}(\mathbf{r}, t)$ have to fulfill Maxwell's equations [20]. Energy conservation for the electromagnetic field is commonly described by Poynting's theorem. We further restrict ourselves to linear, nonmagnetic, and static media, which have a scalar and real permittivity $\epsilon(\mathbf{r})$. Because we are only interested in time-harmonic fields, the time-averaged energy density $\langle w(\mathbf{r}) \rangle_t$ is calculated by

$$\langle w(\mathbf{r}) \rangle_t = \frac{1}{4} [\epsilon(\mathbf{r}) |\mathbf{E}(\mathbf{r})|^2 + \mu_0 |\mathbf{H}(\mathbf{r})|^2]. \quad (9)$$

The vacuum permeability is denoted by μ_0 , and the permittivity is related to the refractive index distribution by $n(\mathbf{r})^2 = \epsilon(\mathbf{r})/\epsilon_0$.

Maxwell's equations can only be solved analytically in a few special cases, for example, if a plane wave is scattered by a sphere or cylinder [21]. For complex scenarios, the electromagnetic fields are usually obtained from numerical solutions of Maxwell's equations. In this study, we use an iterative approach based on a modified Born series [22] to compute the electromagnetic fields in three dimensions for time-harmonic fields with vacuum wavelength λ . This approach is grid based. Therefore, the refractive index distribution in the simulation is discretized by cubic voxels. In all simulations presented in this study, the voxels have a side length of $\lambda/12.5$. To simulate a Lambertian illumination, as described in the previous section, we use 3000 plane waves of a single wavelength λ randomly incident from all directions in the 4π angular space. This approach has been recently used to simulate isotropic illumination to study spatial coherence of light inside scattering media [23]. With the obtained electromagnetic fields, the energy density in the simulation region is calculated with Eq. (9). Averaging over a volume which contains many speckles yields the volume-averaged energy density $\langle w \rangle_t$.

III. RESULTS AND DISCUSSION

A. Dielectric objects with uniform refractive index

According to Yablonoitch, the enhancement of the energy density in sufficiently textured sheets or objects is described by Eq. (1). To verify this dependency with full vectorial electromagnetic simulations, we first consider a cube with a side length of 20λ and a sphere with a diameter of 20λ , which are shown in Figs. 1(a) and 1(b). To texture the surface of the cube, we distributed pyramids with side lengths for the base area equal to λ on one face of the cube. The height of each pyramid was chosen randomly between zero and λ , and consecutive pyramids are nonoverlapping. This textured face was applied to the remaining faces to obtain the textured cube shown in Fig. 1(c). To texture the sphere, we picked 500 points on the surface of the sphere with approximately equal area by applying a Fibonacci grid technique [24]. At each surface point, we positioned a cone with a base diameter of 2λ and a random height between 0.5λ and 2.5λ . As can be seen from Fig. 1, the cones can overlap. All four objects have a uniform refractive index distribution inside their volume and are located in a vacuum. We performed simulations for the different bodies under Lambertian illumination and varied the refractive index inside each object. The refractive indices inside have values between $n = 1.0$ and $n = 2.5$. The

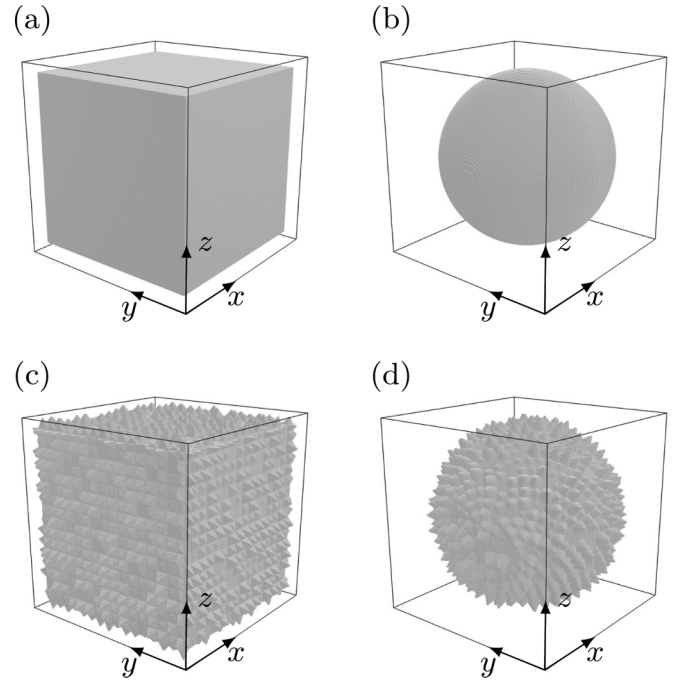


FIG. 1. Objects with smooth surfaces: (a) cube with a side length of 20λ and (b) sphere with diameter of 20λ . Objects with textured surfaces: (c) cube with a side length of 20λ and textured surface modeled by equidistantly spaced pyramids with random height and (d) sphere with diameter of 20λ and textured surface with cones of random height.

electromagnetic fields were used to calculate the energy density distribution $\langle w(\mathbf{r}) \rangle_t / w_0$ with Eq. (9). The energy density distributions for a refractive index of $n = 2.5$ over an xy slice through the middle of the objects are shown in Fig. 2(a). Besides the fast fluctuating nature of the interference patterns, the energy density distribution over the xy slices inside the flat cube and the textured cube is uniform. In contrast, the distribution of the energy density inside a smooth sphere is position dependent. This behavior can be explained even by the radiative transfer theory [11]. The energy density or fluence rate inside a concentric sphere of radius $R_c = (1/n)R_0$ is homogeneous. The radius of this sphere is shown in Fig. 2(a) for the sphere with a smooth surface with a dashed green line. If the smooth sphere is sufficiently textured, the energy density becomes independent of the location inside the sphere, as can be seen in Fig. 2(a). The average internal energy density was calculated by integrating the energy density inside each object and dividing it by its volume. The volume over which the average was performed is shown by the dashed red lines in Fig. 2(a). The normalized average energy densities and the theoretical model described by Eq. (1) are shown in Fig. 2(b). If the surfaces of the cube and the sphere are sufficiently textured the energy density enhancement follows the n^3 law. The energy density distribution becomes independent of the surface shape. The difference in the energy density enhancement for the textured and smooth objects increases with increasing refractive index. The reason for this is that the objects under study have high symmetry and are nonergodic. Therefore, not all modes can be excited from the outside of

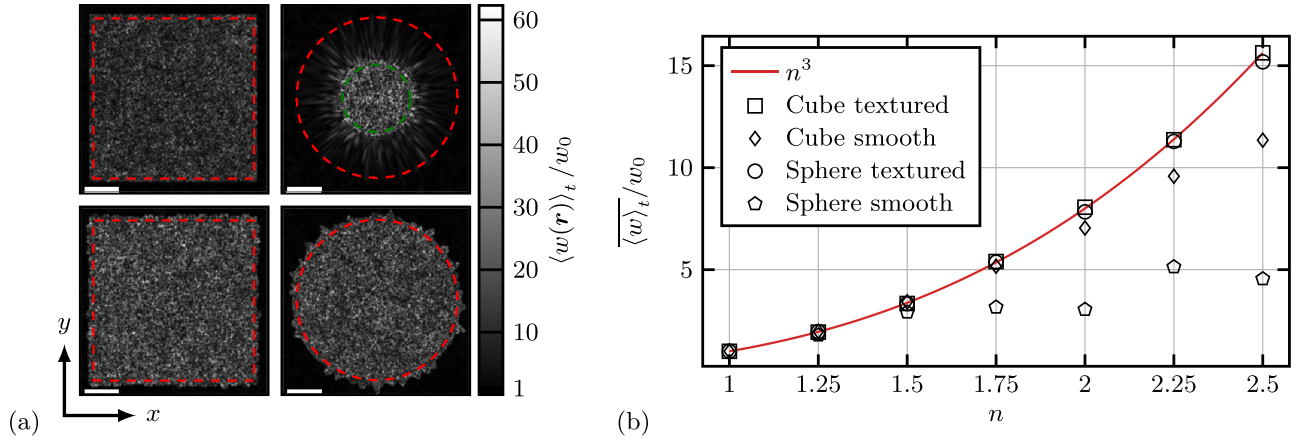


FIG. 2. Lambertian illumination of objects with uniform refractive index distribution. (a) Energy density distributions over xy slices through the middle of the different objects with $n = 2.5$. The left column shows the cubic media and the right column the spherical media (top, smooth surface; bottom, textured surface). The dashed red lines denote the averaging area, and the scale bar is 5λ . The dashed green line denotes the area calculated from the radiative transfer theory in which the energy density is homogeneous. (b) Volume-averaged energy density over the refractive index for the smooth and textured objects. The red line denotes the theoretical enhancement of the energy density.

the objects. In summary, the energy density enhancement for smooth objects depends strongly on the shape of the objects. For small refractive index differences between the object and the surrounding, the deviation to the theoretical model in Eq. (1) becomes smaller for objects with smooth surfaces.

B. Volume scattering dielectrics

In this section, we study the energy density inside volumes filled with dielectric scatterers. In the following, we investigate different scatterer sizes, volume fractions, and refractive indices.

1. Size of the scatterers $< \lambda$

To simulate small scatterers, we chose the smallest possible scatterer volume in our simulations, which is a cubic voxel of our simulation grid. Therefore, the scatterer has sides of length 0.08λ . Since the scattering objects are much smaller than the wavelength, we assume that the shape does not play an important role and that the scattering voxels behave approximately like radiating dipoles but still have a finite amount of volume. This choice makes it possible to investigate volume fractions f_V between zero and 1. In Fig. 3(a), a part of the volume of a typical scattering medium with $f_V = 0.5$, a textured-cubic bounding volume, and refractive indices of $n_1 = 2$ and $n_2 = 1.5$ is shown. In Fig. 3(b) the normalized energy density over an xz slice is shown, where the energy density distribution looks similar to the distribution inside a homogeneous medium [see Fig. 2(a)].

As a first study, we randomly distributed scatterers with refractive index $n_1 = 2$ with different volume fractions inside the four bounding volumes from the previous section. The refractive index of the background medium inside and outside the bounding volume is $n_2 = 1.0$. The average energy density enhancement obtained from the simulations inside the bounding volumes is shown in Fig. 4. For the different bounding volumes $\langle w \rangle_t / w_0$ gives similar results for volume fractions $f_V < 0.8$. Hence, for these volume fractions, the bounding volume is not important because for low concentrations and

the same background refractive index inside and outside the volume, there is no flat surface and for larger concentrations, the volume scattering guarantees equipartition of all modes inside the bounding volume. For $f_V > 0.8$ the results show larger deviations between the smooth and textured bounding volumes. Textured bounding volumes under Lambertian illumination, no matter if it is a sphere or a cube, give similar results as the surface structure guarantees the equipartition of all modes. In the case of smooth bounding volumes, the equipartition of all modes might not be fulfilled, which explains the difference between the enhancement for media with cubic and spherical bounding volumes. If the volume fraction reaches $f_V = 1$, i.e., the scattering diminishes, the results from the previous section are obtained. The results for scattering media composed of small scatterers can be compared to the theoretical model in Eq. (1), where the refractive index n is replaced by the effective refractive index \tilde{n} , which is dependent on the volume fraction. We compare theoretical models with the effective refractive index from the Bruggeman and Maxwell-Garnett effective medium approximations (\tilde{n}_{BG} , \tilde{n}_{MG}) and due to volume averaging over the permittivity

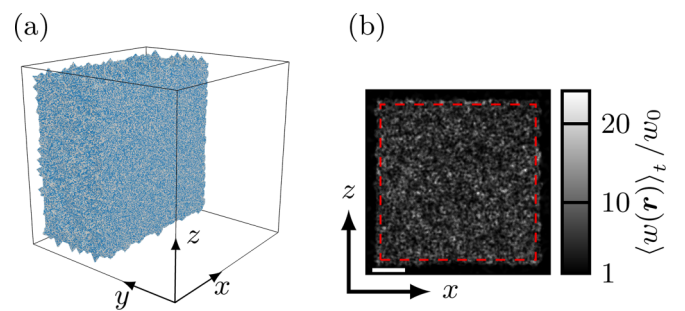


FIG. 3. (a) The clipped volume of the scattering medium with voxel scatterers with side length 0.08λ , $n_1 = 2$ (gray areas), and $f_V = 0.5$. Inside the textured cubic bounding volume, the background medium has a refractive index of $n_2 = 1.5$ (blue areas). (b) The normalized energy density over an xz slice. The dashed red lines denote the averaging area, and the scale bar equals 5λ .

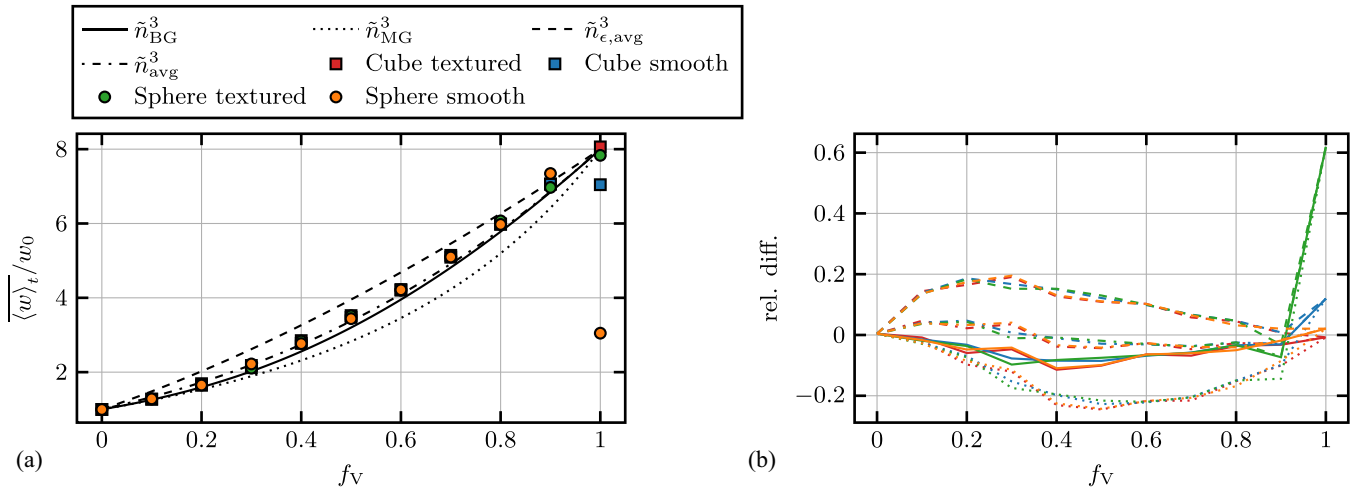


FIG. 4. Volume scattering medium with scatterers smaller than the wavelength and $n_1 = 2$. (a) The average energy density enhancement over the volume fraction f_V for different bounding volumes. The black lines show the different theoretical models. (b) The relative differences for the different bounding volumes to the different theoretical models. The line style denotes the theoretical model and the color denotes the bounding volume type.

distribution $\tilde{n}_{\epsilon,avg}$ and the refractive index distribution \tilde{n}_{avg} . The relative differences between the theoretical models and the simulations is shown in Fig. 4(b). We find that for low concentrations (volume fraction < 0.2) the Bruggeman and Maxwell-Garnett approximations give the best predictions of the energy density enhancement. For larger concentrations, the model of the refractive index averaged effective medium approximation shows the smallest relative differences to the simulation data. In the case of a uniform refractive index, all theoretical models approach the same value. Additionally, we simulated random scatterer distributions with different refractive indices of the scatterers and the background medium inside the bounding volume. To avoid a strong influence of the bounding volume for large scatterer concentrations, as resulted for the cube and sphere with smooth surfaces, we further use the textured cube as a bounding volume. In Fig. 5 the results for three different combinations of scatterer refractive index n_1 and background medium in the bounding volume n_2 are shown. The results for $n_1 = 2.0$ from the previous figure are shown again. The refractive index outside the bounding volume is 1.0. For all three scenarios, the average energy density enhancement can be well approximated with the third power of the refractive index and an effective medium theory. As before, the average over the refractive index matches the simulations best over the full range of concentrations. For small refractive index contrasts, the difference between the effective medium approximations becomes smaller as can be seen for the cases of $n_1 = 2.0, n_2 = 1.0$ and $n_1 = 2.0, n_2 = 1.5$.

2. Size of the scatterers $\geq \lambda$

Further, we increased the size of the single scatterers. In the following, the scatterers have a spherical shape and a diameter of $d = \lambda$, and $d = 5\lambda$. To generate the scattering medium, we calculated the positions of a face-centered-cubic packing and removed randomly a certain number of points. Indeed, the positions of the remaining points are still heavily correlated, but this type of approach makes it easy to distribute

spheres up to a volume fraction of $f_V \approx 0.74$. The spheres with n_1 were positioned at the remaining grid points and afterwards cropped by the bounding volume of the textured cube. Illustrations of two scattering media with $f_V \approx 0.5$ are shown in Figs. 6(a) and 6(c) for spheres with $d = \lambda$ and $d = 5\lambda$, respectively. The true volume fraction occupied by the scatterers was calculated by averaging over the volume, which was also used for calculating the average energy density enhancement. In Figs. 6(b) and 6(d) the energy density over an xz slice is given, where the dashed red lines show the margin of the averaging area. From the energy density

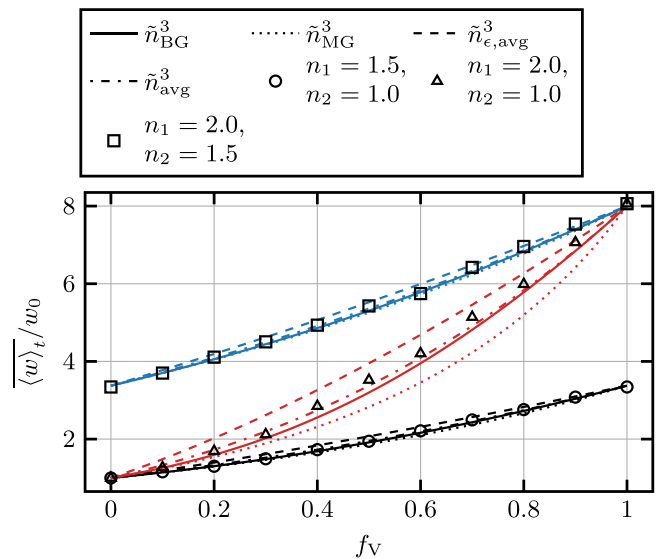


FIG. 5. Scattering media composed of small scatterers with different refractive indices of the scatterer n_1 and the background medium n_2 . The refractive index outside the bounding volume is 1.0. The line colors of the theoretical models are assigned as follows: black, $n_1 = 1.5, n_2 = 1.0$; red, $n_1 = 2.0, n_2 = 1.0$; and blue, $n_1 = 2.0, n_2 = 1.5$.

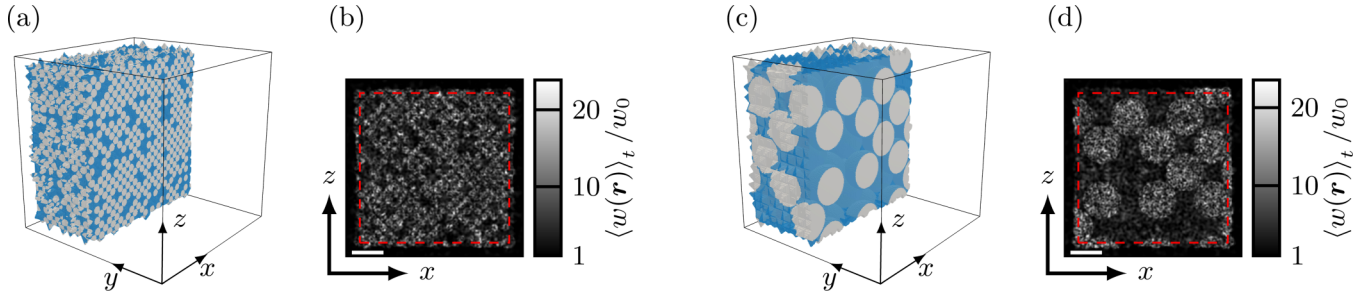


FIG. 6. Clipped volumes of two scattering media with $n_1 = 2.0$, $n_2 = 1.5$ are shown in (a) and (c). Both have $f_V \approx 0.5$ volume concentration of the scatterers. The diameter of a single scatterer is (a) λ and (b) 5λ . The normalized energy densities over an xz slice are shown in (b) for $d = \lambda$ and in (d) for $d = 5\lambda$. The dashed red lines denote the averaging area, and the scale bars equal 5λ .

distributions in the figure one can still anticipate the locations of the spherical scatterers. Inside the scatterers the energy density is enhanced due to the larger refractive index. This can be seen especially for the large scatterers in Fig. 6(d). The volume-average energy density enhancement inside the whole scattering media for different volume fractions, refractive indices, and diameters is shown in Fig. 7. As we only simulated one scattering medium for each parameter set, the average energy density can strongly depend on the configuration of the scatterer positions. In particular, this is the case for large scatterers and low volume fractions, as there are only a few scatterers distributed inside the medium. To estimate the variation of the averaged energy density over the total volume, we additionally calculated the averaged energy density over eight nonoverlapping subvolumes. Each of these subvolumes can have different volume fractions. The data points for the subvolumes are shown in the top panels in Fig. 7 as red and blue semitransparent circles. In addition to the theoretical models based on effective medium approximations, the theoretical estimate due to the work of Yablonoivitch for an inhomogeneous dielectric medium is also shown [Eq. (4)],

which is denoted by w_{lim} . The relative differences between the normalized energy density averaged over the total medium and the theoretical models is shown in the bottom panels of Fig. 7. The results for scatterers of size $d = \lambda$ show the overall best agreement for the theoretical model with $\tilde{n}_{\epsilon, \text{avg}}$, only for concentration $f_V > 0.6$ the averaged energy density is better described by the \tilde{n}_{avg} model in the case of $n_1 = 2.0$, $n_2 = 1.0$ and by the model w_{lim} in the case of $n_1 = 2.0$, $n_2 = 1.5$. This deviation might be due to resonances in the overall configuration of the spheres for a discrete volume fraction. In general the energy densities in the subvolumes do not fluctuate strongly, as can be seen by the semitransparent red circles in Fig. 7. For spherical scatterers with diameter $d = 5\lambda$ the average energy density enhancement for the three different refractive index combinations cannot be described well by one theoretical model. Due to the large scatterers, the averaged energy densities inside the subvolumes fluctuate. Especially for small volume concentrations only a small number of scatterers are inside the medium; therefore, certain subvolumes can have $f_V \approx 0$. Nevertheless, the majority of data points lie within the w_{lim} model as an upper bound and

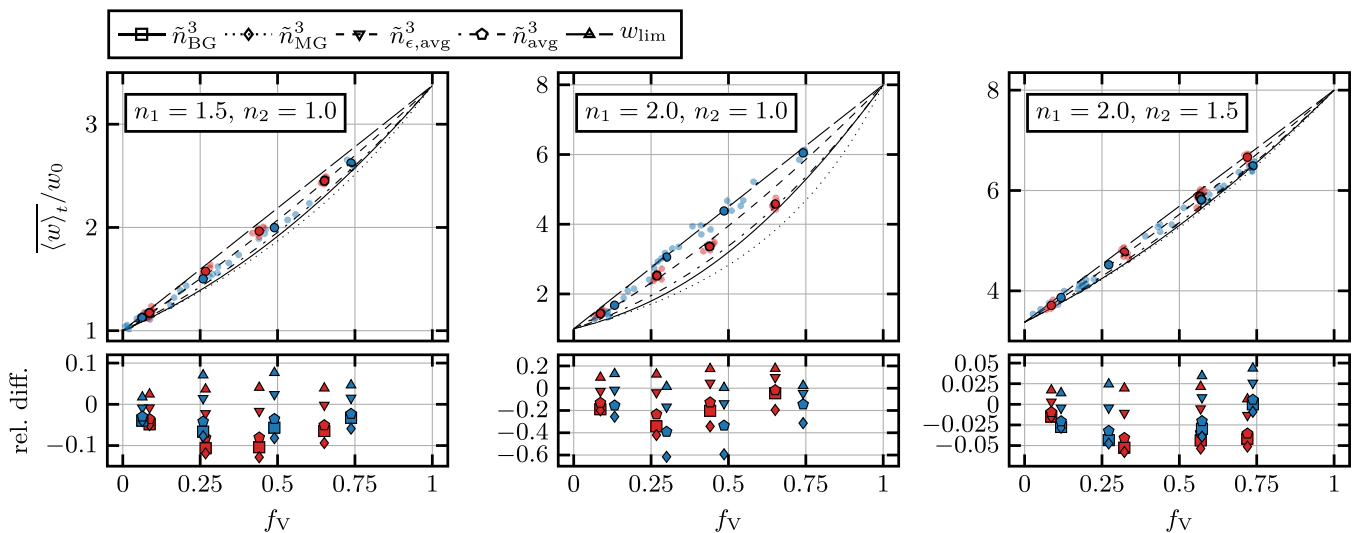


FIG. 7. Average energy density inside various media with different volume fractions f_V consisting of spherical scatterers with diameter $d = \lambda$ (red color) and $d = 5\lambda$ (blue color). The top panels show the normalized average energy density $\langle w \rangle_t / w_0$ for three different combinations of n_1 and n_2 . Solid circles with black edges show the mean over the total volume and the semitransparent circles show averages of subvolumes. The bottom panels show the relative differences over f_V of $\langle w \rangle_t / w_0$ averaged over the total volumes to the different theoretical models.

\tilde{n}_{BG} as a lower bound. For large scatterers, we expect that the average energy density can be modeled by w_{lim} . As the results for $d = 5\lambda$ do not show this behavior for all simulated media we conclude that the scattering areas are still too small and that resonances of the spherical scatterers might have a large effect on the average energy density.

IV. CONCLUSION

In this study, we investigated the monochromatic Lambertian illumination of dielectric media of size scales of tens of wavelengths. For uniform refractive indices, we validated the known average energy density enhancement of n^3 for sufficiently textured objects with full vectorial numerical solutions of Maxwell's equations in three dimensions. We found that the energy density is homogeneously distributed inside the textured objects, if the fast fluctuating nature of the interference patterns is not considered. In non-ergodic systems, such as a sphere, this might not be the case. These results are also obtained from radiative transfer theory [11].

We further simulated scattering media composed of scatterers much smaller than the wavelength and showed that the average energy density enhancement can be estimated with an effective refractive index \tilde{n} depending on the volume fraction by calculating \tilde{n}^3 . We performed simulations for different refractive indices of the scatterers and the refractive index of the background medium inside the bounding volume. Simulations for volume fractions from zero to unity showed that for $f_v < 0.8$ the results are independent of the bounding volume but for larger concentrations the averaged energy density of the smooth bounding volumes shows deviations from the \tilde{n}^3 model. Further simulations with concentrations between $f_v = 0.9$ and unity need to be performed to show that there is also a discontinuity for the electromagnetic theory between the low-scattering ($f_v < 1$) and the nonscattering ($f_v = 1$) case. This discontinuity is present in the radiative transfer theory [11,25]. Furthermore, we found that for our simula-

tions the best predictions of the average energy density inside the medium for all volume fractions can be made with an effective refractive index calculated by volumetric averaging over the refractive index \tilde{n}_{avg} . For small scatterers $< \lambda$, our study shows the possibility to obtain the effective refractive index from the electromagnetic near fields inside a scattering medium under Lambertian illumination by calculating $(\langle w \rangle_i / w_0)^{1/3}$. This could be tested in future studies comparing different methods to obtain the effective refractive index from electromagnetic near-field simulations inside scattering media [26].

For spherical scatterers with diameter λ , the average energy density enhancement can be well described with the effective medium approach $\tilde{n}_{\epsilon,avg}^3$. This confirms the choice of the effective medium approach in our recent publications [12,13], where similar scatterers and low concentrations were used. Only for large concentrations this model deviates from the simulation results. The results for scattering media composed of scatterers with diameter $> \lambda$ cannot be consistently described by one model but for $n_1 = 2.0$, $n_2 = 1.5$ the average energy density shows a tendency to be described with w_{lim} . Nevertheless, the size of a single scatterer might still be too small for Eq. (4) to be valid. Future simulations should be performed to extend and confirm the outcomes of this work. For example, the simulation volume used for averaging should be enlarged or the averaging should be performed over many configurations. Due to the increasing speed and memory capacity of computer systems this should be feasible in the near future.

ACKNOWLEDGMENTS

We would like to thank Dr. Benjamin Krüger for the development of the numerical algorithm. This work was supported by the Deutsche Forschungsgemeinschaft (DFG, German Research Foundation) under Project No. 445978371. F.O. acknowledges financial support from the Evangelisches Studienwerk Villigst e. V.

-
- [1] V. Ntziachristos, Going deeper than microscopy: The optical imaging frontier in biology, *Nat. Methods* **7**, 603 (2010).
 - [2] A. Polman and H. A. Atwater, Photonic design principles for ultrahigh-efficiency photovoltaics, *Nat. Mater.* **11**, 174 (2012).
 - [3] A. Kienle and F. Foschum, 250 years lambert surface: Does it really exist? *Opt. Express* **19**, 3881 (2011).
 - [4] E. Yablonovitch and G. D. Cody, Intensity enhancement in textured optical sheets for solar cells, *IEEE Trans. Electron Devices* **29**, 300 (1982).
 - [5] Z. Yu, A. Raman, and S. Fan, Fundamental limit of nanophotonic light trapping in solar cells, *Proc. Natl. Acad. Sci. U.S.A.* **107**, 17491 (2010).
 - [6] S. Blanco and R. Fournier, An invariance property of diffusive random walks, *Europhys. Lett.* **61**, 168 (2003).
 - [7] K. Case and P. Zweifel, *Linear Transport Theory*, Addison-Wesley Series in Nuclear Engineering (Addison-Wesley, Reading, MA, 1967).
 - [8] R. Pierrat, P. Ambichl, S. Gigan, A. Haber, R. Carminati, and S. Rotter, Invariance property of wave scattering through disordered media, *Proc. Natl. Acad. Sci. U.S.A.* **111**, 17765 (2014).
 - [9] R. Savo, R. Pierrat, U. Najar, R. Carminati, S. Rotter, and S. Gigan, Observation of mean path length invariance in light-scattering media, *Science* **358**, 765 (2017).
 - [10] F. Tommasi, L. Fini, F. Martelli, and S. Cavalieri, Invariance property in inhomogeneous scattering media with refractive-index mismatch, *Phys. Rev. A* **102**, 043501 (2020).
 - [11] F. Martelli, F. Tommasi, L. Fini, L. Cortese, A. Sassaroli, and S. Cavalieri, Invariance properties of exact solutions of the radiative transfer equation, *J. Quant. Spectrosc. Radiat. Transfer* **276**, 107887 (2021).
 - [12] F. Ott, B. Krüger, A. Liemert, and A. Kienle, Energy density distribution of light inside two-dimensional randomly scattering slabs illuminated by a plane wave, *J. Quant. Spectrosc. Radiat. Transfer* **235**, 40 (2019).

- [13] F. Ott, D. Reitzle, B. Krüger, A. Liemert, and A. Kienle, Distribution of light inside three-dimensional scattering slabs: Comparison of radiative transfer and electromagnetic theory, *J. Quant. Spectrosc. Radiat. Transfer* **277**, 107987 (2022).
- [14] L. Landau and E. Lifshitz, *Electrodynamics of Continuous Media*, Course of Theoretical Physics Vol. 8 (Pergamon, New York, 1960).
- [15] E. Yablonovitch, Statistical ray optics, *J. Opt. Soc. Am.* **72**, 899 (1982).
- [16] T. C. Choy, *Effective Medium Theory: Principles and Applications*, Vol. 165 (Oxford University Press, Oxford, 2015).
- [17] V. A. Markel, Introduction to the Maxwell-Garnett approximation: Tutorial, *J. Opt. Soc. Am. A* **33**, 1244 (2016).
- [18] P. Yazhgur, G. J. Aubry, L. S. Froufe-Pérez, and F. Scheffold, Light scattering from colloidal aggregates on a hierarchy of length scales, *Opt. Express* **29**, 14367 (2021).
- [19] D. Werdehausen, X. G. Santiago, S. Burger, I. Staude, T. Pertsch, C. Rockstuhl, and M. Decker, Modeling optical materials at the single scatterer level: The transition from homogeneous to heterogeneous materials, *Adv. Theory Simul.* **3**, 2000192 (2020).
- [20] J. D. Jackson, *Classical Electrodynamics* (American Association of Physics Teachers, College Park, MD, 1999).
- [21] C. F. Bohren and D. R. Huffman, *Absorption and Scattering of Light by Small Particles* (Wiley, New York, 2008).
- [22] B. Krüger, T. Brenner, and A. Kienle, Solution of the inhomogeneous Maxwell's equations using a Born series, *Opt. Express* **25**, 25165 (2017).
- [23] M. Leonetti, L. Pattelli, S. De Panfilis, D. S. Wiersma, and G. Ruocco, Spatial coherence of light inside three-dimensional media, *Nat. Commun.* **12**, 4199 (2021).
- [24] R. Swinbank and R. J. Purser, Fibonacci grids: A novel approach to global modelling, *Q. J. R. Meteorol. Soc.* **132**, 1769 (2006).
- [25] M. Majic, W. R. C. Somerville, and E. C. Le Ru, Mean path length inside nonscattering refractive objects, *Phys. Rev. A* **103**, L031502 (2021).
- [26] D. Mackowski and M. I. Mishchenko, Direct simulation of extinction in a slab of spherical particles, *J. Quant. Spectrosc. Radiat. Transfer* **123**, 103 (2013).